DOI: 10.1002/cbic.200900001

Selectivity of Competitive Multivalent Interactions at Interfaces

Thomas André,[a, e] Annett Reichel,[b] Karl-Heinz Wiesmüller,[c] Robert Tampé,[b] Jacob Piehler,*[b] and Roland Brock*[a, d]

The development of synthetic, low-molecular-weight ligand receptor systems for the selective control of biomolecular interactions remains a major challenge. Binding of oligohistidine peptides to chelators containing Ni^{2+}-loaded nitrilotriacetic acid (NTA) moieties is one of the most widely used and best-characterised recognition systems. Recognition units containing multiple NTA moieties (multivalent chelator headgroups, MCHs) recognise oligohistidines with substantially increased binding affinities. Different multivalencies both at the level of the MCH and at that of the oligohistidine ligand provide a powerful means to vary the affinity of the interaction systematically. Here we have explored the selectivity for the binding of different oligohistidines to immobilised MCH. Using microarrays of mono-, bis-, tris- and tetrakis-NTA chelators spotted at different surface densities, we explored the ability of these binders to discriminate fluorescently labelled hexa- and decahistidine peptides. When hexa- and decahistidine were tested alone, the discrimination of ligands showed little dependence either on the nature or on the density of the chelator. In contrast, coincubation of both peptides decreased the affinity of hexahistidine, increased the affinity of decahistidine, and made the binding of decahistidine highly dependent on MCH density. Kinetic binding assays by dual-colour total internal reflection fluorescence spectroscopy revealed active exchange of His_6 by His_{10} and confirmed the high selectivity towards His_{10}. Our results establish the key role of surface multivalency for the selectivity of multivalent interactions at interfaces.

Introduction

Multivalency is a highly versatile phenomenon for the generation and control of specific, noncovalent molecular interactions, that is frequently employed in nature for, for example, the recognition of carbohydrates.[1] By covalently linking together of two or more copies of a ligand, as well as its receptor, the binding constants of low-affinity interactions can be increased by several orders of magnitude.[2] Although multivalent design is a powerful approach for increasing molecular binding affinities, the molecular mechanisms that govern the specificities of multivalent interactions are still poorly understood.[3,4] This holds particularly true for multivalent interactions at surfaces, where molecular multivalency is combined with multivalency resulting from the potential to interact simultaneously with multiple binding partners attached to a surface.[5–8]

Binding of oligohistidine peptides to chelators containing Ni^{2+}-loaded nitrilotriacetic acid (NTA) moieties is a highly versatile, low-molecular-weight recognition system in which multivalency has been exploited for control of binding affinities. Interactions with oligohistidines may be controlled through complexation of Ni^{2+} ions and competition with imidazole. We have recently introduced multivalent chelator headgroups (MCHs, Scheme 1 A), which bind oligohistidines with substantially increased binding affinities relative to the individual NTAs.[9] The affinity of the interaction may be systematically changed by variation of the multivalency, both of the oligohistidine ligand as well as of the chelator.[9] Although the interaction of individual receptor ligand pairs in this system has been studied in great detail, little is known about the ability to discriminate different ligands.

Here we have systematically explored the abilities of bis-, tris- and tetrakis-NTA systems immobilised at different densities on glass surfaces to discriminate oligohistidine peptides of different lengths.

In this recognition system, multivalency may be varied in different ways: the different multichelator headgroups and the

[a] Dr. T. André, Prof. Dr. R. Brock
Department of Molecular Biology, Interfaculty Institute for Cell Biology
University of Tübingen
Auf der Morgenstelle 15, 72076 Tübingen (Germany)

[b] A. Reichel, Prof. Dr. R. Tampé, Prof. Dr. J. Piehler
Institute of Biochemistry, Johann Wolfgang Goethe University
Max-von-Laue-Strasse 9, 60438 Frankfurt/Main (Germany)
E-mail: piehler@biologie.uni-osnabrueck.de

[c] Prof. Dr. K.-H. Wiesmüller
EMC microcollections GmbH
Sindelfinger Strasse 3, 72070 Tübingen (Germany)

[d] Prof. Dr. R. Brock
Department of Biochemistry, Nijmegen Centre for Molecular Life Sciences
Radboud University Nijmegen, Medical Centre (Route 286)
PO Box 9101, 6500 HB Nijmegen (The Netherlands)
Fax: (+31) 24-3616413
E-mail: r.brock@ncmls.ru.nl

[e] Dr. T. André
Present address: Bachem AG
Hauptstrasse 144, 4416 Bubendorf (Switzerland)

Supporting information for this article is available on the WWW under http://dx.doi.org/10.1002/cbic.200900001: EC_{50} values for competitive binding of His_6 and His_{10} peptides, the optimisation of surface chemistry, the validation of the stopped-flow protocol for titration with imidazole, as well as the evaluation of the influence of the fluorophores on the dissociation and the presence of fluorescence resonance energy transfer.

 © 2009 Wiley-VCH Verlag GmbH & Co. KGaA, Weinheim

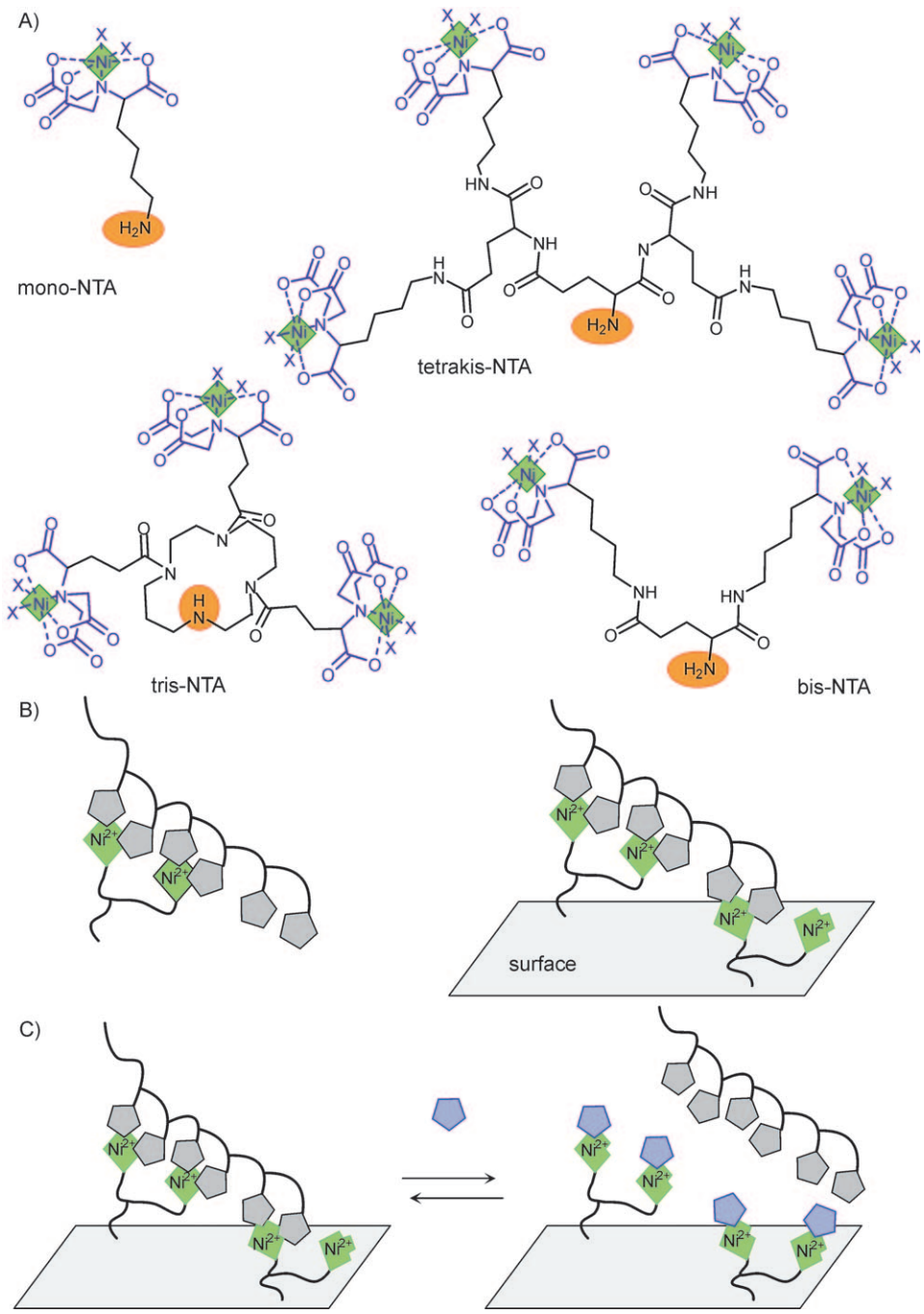

Scheme 1. A) Molecular structures of mono-NTA and bis-, tris- and tetrakis multivalent chelator headgroups (MCHs). X's denote coordination sites for histidine side chains within the chelating sites, while amino groups for surface immobilisation are highlighted by ovals. B) Schematic representation of the interaction of hexahistidine with bis-NTA in solution (left) and on surfaces (right). These different types of multivalencies are referred to as "molecular multivalency" and "surface multivalency". C) Dissociation of surface binding in the presence of the monovalent competitor imidazole.

two oligohistidine peptides possess different degrees of "molecular multivalency", whereas immobilisation of the MCHs at different densities enables variation of "surface multivalency" (Scheme 1 B). We reasoned that variation of degrees of surface multivalency in combination with different degrees of molecular multivalency should provide a powerful means for creating selectivity for the recognition of different ligands. Through the ability to vary multivalency systematically in a controlled manner, moreover, we expected to gain further insight into multivalent interaction at interfaces in general. In particular, through the use of two oligohistidine peptides of different lengths our analyses focused on the mutual competition of ligands of different multivalency. In line with previous experiments,[10,11] we focused on hexa- and decahistidines, which are both used as affinity tags for the purification of recombinant proteins and clearly show distinguishable binding characteristics to MCHs.[8,10] Equilibrium binding of fluorescently labelled His_6 or His_{10} peptides alone or in combination was probed by using microarrays of mono-, bis-, tris- and tetrakis-NTA immobilised in different densities.

Previously we have employed the titration of fluorescently labelled ligands on microarrays functionalised with a low-molecular-weight recognition molecule for the determination of binding constants.[12] In a subsequent work, for a bivalent ligand, we observed a dependence of affinity on receptor density.[13] These previous results demonstrated the potential of microarrays for quantitative analysis of receptor–ligand interactions, and more specifically multivalent interactions. For analysis of the interactions of oligohistidines with the MCHs, instead of titration of the arrays with ligand, equilibrium binding of the ligands was first established, followed by stepwise titration with the monovalent inhibitor imidazole, which is commonly used to induce dissociation of oligohistidines from NTA chelators.

Moreover, the binding kinetics of His_6- and His_{10}-tagged proteins were characterised by total internal reflection fluorescence spectroscopy (TIRFS). TIRFS has been frequently employed to measure time-resolved binding of fluorescent molecules to surfaces. The principle of total internal reflection very

 © 2009 Wiley-VCH Verlag GmbH & Co. KGaA, Weinheim

effectively restricts the detection to surface-bound molecules.[14,15] Through the use of dual-colour TIRFS detection, we independently monitored association and dissociation of both His_6- and His_{10}-tagged proteins in real time. Our results demonstrate that a substantial selectivity towards His_{10} relative to His_6 can be achieved by optimisation of molecular and surface multivalencies.

Results

Generation of MCH density microarrays

To explore the roles of molecular and surface multivalencies we manufactured MCH density arrays. The NTA chelators were coupled to the surface through reactions of the amino groups present in each compound (Scheme 1) with surface epoxy groups or carboxylic acid *N*-hydroxysuccinimidyl (NHS) esters. A piezo-driven nanopipettor was used to pipette sub-nanoliter volumes of NTA solutions. Surface immobilisation by nanopipetting is subject to experimental constraints very different from those associated with immobilisation by homogeneous incubation of surfaces. It is a specific challenge to ensure homogeneous surface functionalisation in the presence of drying of the spots. Highly homogeneous functionalisation of spots was achieved by spotting chelator solutions on surfaces activated through coupling of a homobifunctional succinimidyl ester linker on amino-functionalised glass surfaces (Figure S1 in the Supporting Information).[19] We did not include an explicit quenching of residual succinimidyl esters in our functionalisation protocol because the surfaces were washed intensively after pipetting of MCHs, and succinimidyl esters are subject to rapid proteolysis in aqueous buffers. The specificity of the binding of oligohistidines to the MCHs was validated by incubation of the MCHs in the presence of EDTA, which complexes Ni^{2+} ions (Figure S2).

Titration curves of individual oligohistidine peptides

The strengths of interactions of oligohistidine peptides with the MCHs were compared on the basis of EC_{50} values for titration with the monovalent competitor imidazole (Scheme 1 C). MCH arrays were incubated with a fluorescently labelled oligohistidine, followed by stepwise titration with imidazole. Microarray substrates were mounted in an open sample holder and arrays were scanned after mixing and incubation by use of a confocal laser scanning microscope. The buffer containing the fluorescent ligand was left on the array in order to ensure equilibrium conditions. This protocol followed a previously published procedure for the determination of dissociation constants.[12] The time required to reach equilibrium after addition of competitor was first determined by a stopped-flow protocol. About 3 min after addition of imidazole, about 80% of the equilibrium dissociation had been reached. Dissociation of the remaining 20% was slow and constant over a further 30 min (Figure S3). For this reason, scanning of the array 5 min after each addition of competitor was chosen as a reasonable compromise between duration of an experiment and formation of equilibrium. In order to enable a direct visual comparison of EC_{50} values and the steepness of the curves, residual background was subtracted from the titration curves (Figure S4) and the curves were normalised on the basis of the intensities in the absence of imidazole. Carboxyfluorescein and the Cy5-like dye S0387 were selected as fluorophores for the labelling of oligohistidine peptides.[20] By labelling both oligohistidine peptides with either fluorophore, we ascertained that the fluorophores were without influence on the binding affinities (Figure S5).

With four MCHs spotted at seven different concentrations each, 28 binding curves were obtained simultaneously (Figure 1 A). The normalised titration curves were fitted by use of a logistic sigmoidal function [Eq. (1)]. EC_{50} values for the titration with imidazole varied from 0.8 mM to 16.6 mM. The lowest EC_{50} value was found for His_6 on mono-NTA (not shown), and the highest for His_{10} on tris-NTA (Figure 1 B). After the titration, some spots were still visible, most probably due to unspecific binding of peptide. For mono-NTA, binding was only a little above background at low chelator densities. Only for the highest mono-NTA densities could titration curves be determined reliably, precluding an analysis of the density dependence. This chelator was therefore excluded from further analyses.

As reported previously, EC_{50} values increased with increasing molecular multivalency on going from bis- to tris-NTA.[9] Surprisingly, in contrast to this dependence on molecular multivalency, the EC_{50} values were largely independent of the density

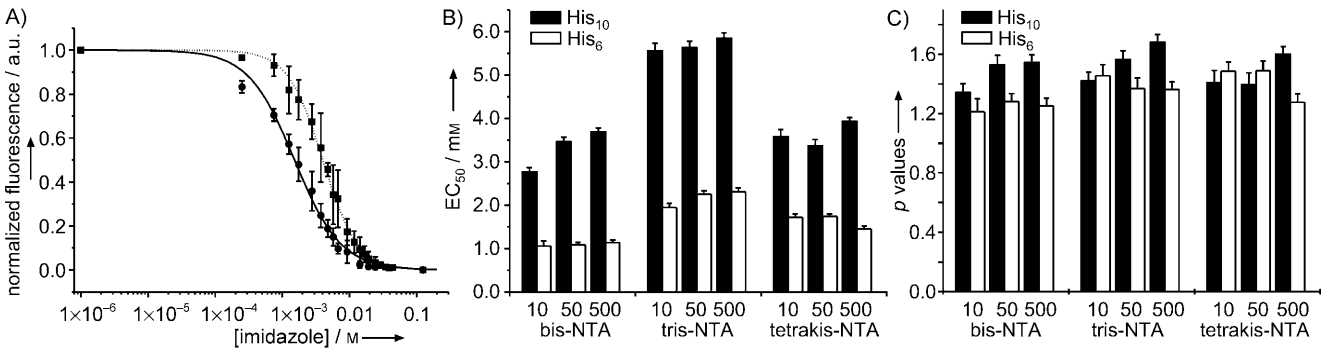

Figure 1. Imidazole titration of His_6 and His_{10} from MCH microarrays. A) Representative titration curves for His_6 (●) and for His_{10} (■) fitted with Equation (1) for binding to tetrakis-NTA spotted at a concentration of 500 μM. Summary of B) EC_{50} values and C) *p* values for His_6 and His_{10} on MCH microarrays (MCHs spotted from 10 to 500 μM solutions).

 © 2009 Wiley-VCH Verlag GmbH & Co. KGaA, Weinheim

of chelator on the surface. Only on bis-NTA was some density dependence observed for His_{10}. More or less uniformly, the EC_{50} values for His_{10} were larger than those for His_6 by a factor of 2 to 2.5. The rather small differences in EC_{50} values for His_6 versus His_{10} are consistent with the results obtained by isothermal titration calorimetry (ITC), which for His_{10} had also yielded K_D values that were only slightly lower than those for His_6.[9] However, the differences were smaller than those obtained for the imidazole-induced dissociation of oligohistidine-tagged proteins from immobilised MCHs measured in a flow system.[10]

In addition, the titration curves are characterised by their *p* values, which relate to the steepness of the curves. The larger the *p* value, the smaller the concentration range of imidazole over which dissociation of the oligohistidine from the chelators was induced. For His_{10}, there were slight positive correlations with chelator density for bis-, tris- and tetrakis-NTA, whereas for His_6 a negative correlation was observed for tris- and tetrakis-NTA (Figure 1 C).

Simultaneous titration of His_6 and His_{10}

The individual titrations had revealed only minor differences in the various MCHs towards the imidazole-induced release of different oligohistidine ligands. In order to establish discriminatory capabilities of MCHs towards different oligohistidine peptides directly, MCH microarrays were incubated simultaneously with His_6 and His_{10} labelled with S0387 and carboxyfluorescein, respectively. The combination of carboxyfluorescein and S0387 maximised the spectral separation of the two fluorophores, thereby avoiding quenching of the short-wavelength dye by fluorescence resonance energy transfer (FRET, Figure S6).

At the onset of the titration, both ligands were present on all spots (Figure 2). Nevertheless, for the tetrakis-NTA spots, relative to the other chelators, a pronounced preference for binding of the fluorescein-labelled decahistidine peptide was apparent from the strong fluorescence in the green channel. For all spots, titration with imidazole led to a preferential initial dissociation of the S0387-labelled His_6, resulting in a selective enrichment of His_{10} on the microarray (Figure 3). Both peptides were used at the same concentration. Still, it was impossible to quantify the enrichment of either molecule in absolute terms. The instrument settings for the detection of fluorescence were adjusted so that roughly similar signals were detected in both channels and signals with sufficiently high signal-to-noise ratios could be recorded over the whole range of imidazole concentrations.

In the presence of His_{10}, the imidazole concentrations required to induce release of His_6 were significantly lower than those required when His_6 was present alone (for example, 0.6 mM versus 1.1 mM for bis-NTA at a spotted concentration

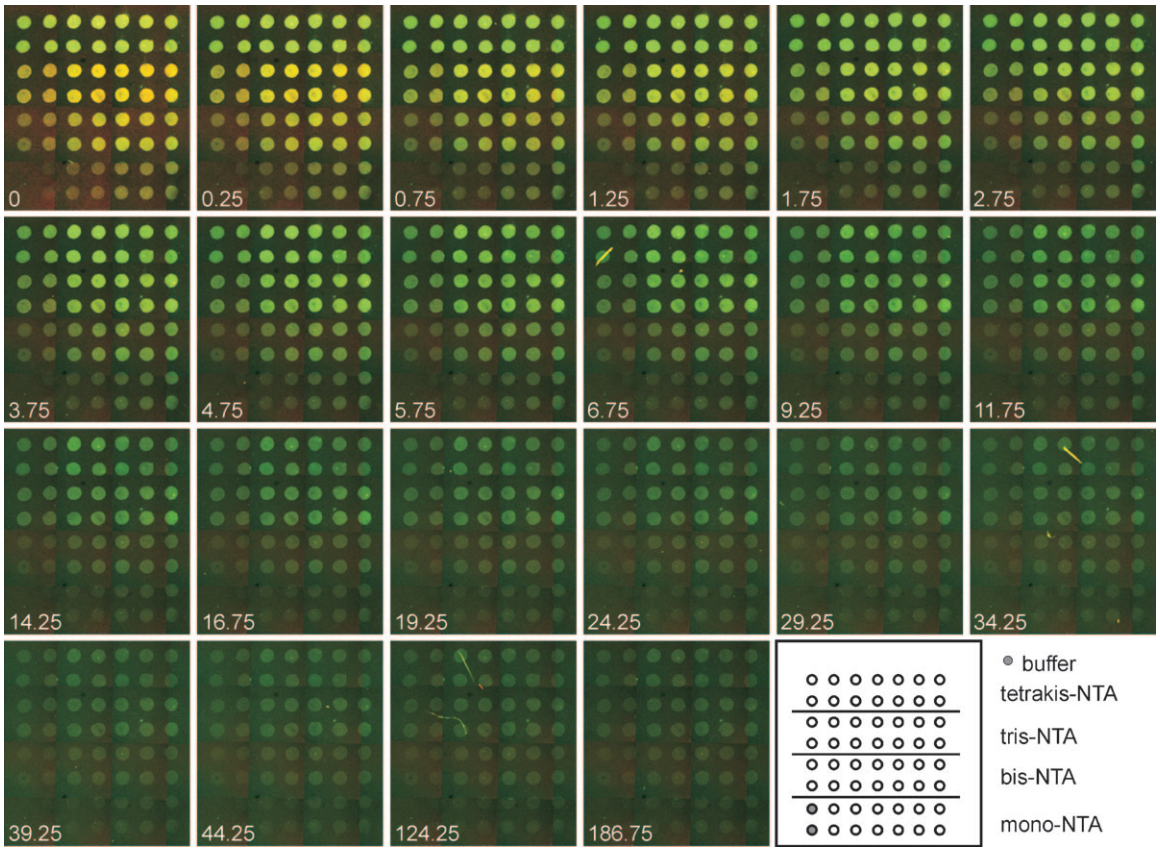

Figure 2. Simultaneous detection of imidazole-induced dissociation of fluorescently labelled oligohistidines from MCH microarrays. Microarrays were incubated with Fluo-Ahx-His_{10}-OH and S0387-Ala_2-His_6-OH (20 nM), and imidazole was added to the final concentrations [mM] indicated in each panel (Fluo: 5(6)-carboxyfluorescein; OH indicates a free C terminus, Ahx: 6-aminohexanoic acid). The layout of the MCH array is depicted in the bottom right corner: Concentrations of spotted MCHs increase from left to right (2.5, 5, 10, 25, 50, 100, 500 μM). For mono-NTA concentrations were higher by a factor of 2.5.

 © 2009 Wiley-VCH Verlag GmbH & Co. KGaA, Weinheim

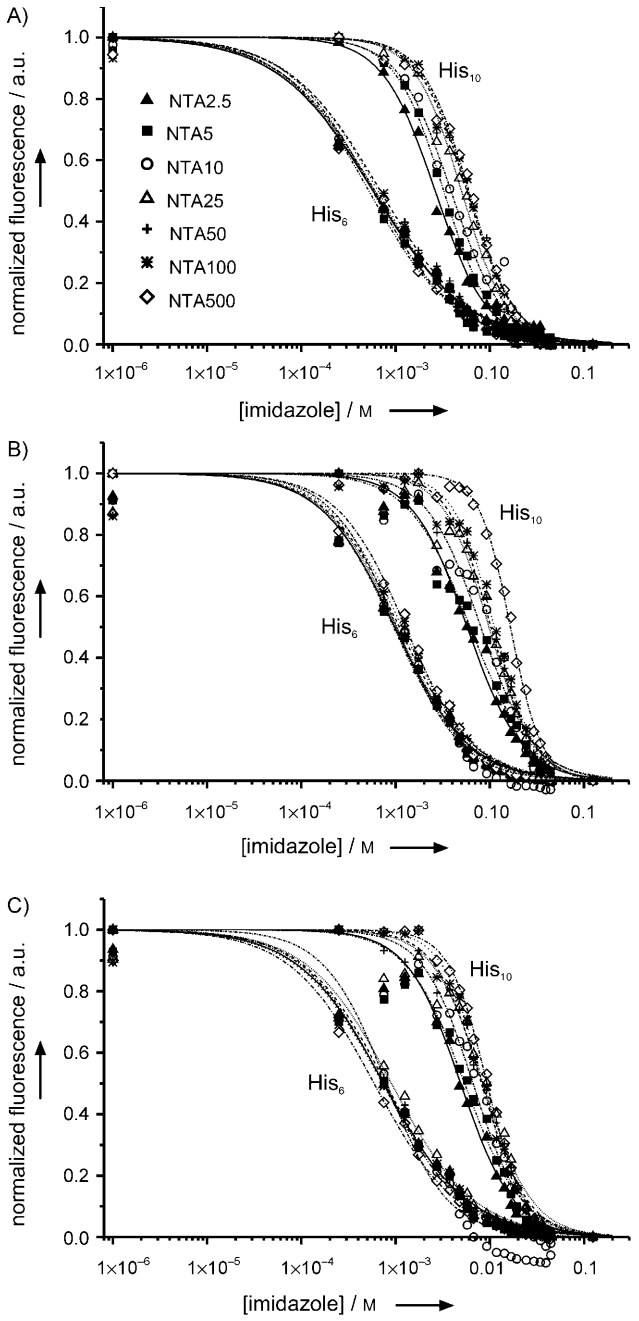

Figure 3. Normalised imidazole-induced dissociation curves for competitive binding of His_6 and His_{10}. A) Dissociation from bis-NTA, B) from tris-NTA, and C) from tetrakis-NTA. The residual net fluorescence on each spot at the end of the titration was set to zero, the net fluorescence on each spot at the beginning of the titration to 1.0.

of 500 μM, and 1.3 mM versus 2.3 mM for tris-NTA at the same spotted concentration). In remarkable contrast, for His_{10} in the presence of His_6 the EC_{50} values were higher than those determined for His_{10} alone.

In addition, the simultaneous presence of both oligohistidine ligands had an unexpected effect on the dependence of EC_{50} values for decahistidine on chelator density (Figure 4). For His_{10}, the EC_{50} values were now strongly density dependent for all chelators, this density dependence being most pronounced for tris-NTA. In contrast, for His_6, similarly to the titration of this peptide alone, the density of the chelator had little influence on the EC_{50} values. Only for tris-NTA was a slight positive dependence on chelator density observed.

The *p* values were affected in a similar fashion. For His_6, a uniform decrease in *p* values was observed, corresponding to weaker slopes, whereas for His_{10} the *p* values for the dissociation from bis-NTA were slightly increased. For tetrakis- and, especially, tris-NTA the positive correlation of *p* values with chelator density was strongly increased. In order to ascertain that the changes in EC_{50} values were not due to interaction of the fluorophores, we confirmed that the shift in the EC_{50} values was also observed when one of the ligands was not fluorescently labelled (not shown).

Discrimination of oligohistidine ligands

The simultaneous measurements of the dissociation of His_6 and His_{10} had revealed that the dissociation behaviour of either His_6 or His_{10} on the NTA multichelator headgroups is strongly influenced by the presence of the corresponding other ligand. When both ligands were present, the differences in EC_{50} and *p* values were more pronounced, and both values depended more strongly on the nature and density of the MCH. Thus, the discriminatory abilities of the different MCHs for the two oligohistidine ligands are significantly larger than suggested by the individual measurements. To compare the selectivity afforded by the different chelators and chelator densities in more detail we calculated the ratios of EC_{50} values for His_{10} and His_6 (Figure 5). With respect to the EC_{50} values, the selectivity increased with the valency and the density of the chelator head. For His_{10} on tetrakis-NTA, EC_{50} values were higher than those for His_6 by factors of up to 15.

Competition kinetics in a flow system

The puzzling outcome of the competitive binding experiments in which both ligands were present simultaneously was that, upon competitive binding, the EC_{50} values for His_6 and His_{10} were shifted in opposite directions (relative to the situation in noncompetitive binding). The extents of these shifts correlated positively with chelator density. In order to unravel the molecular mechanism underlying the mutual influence of the surface binding affinities of His_6 and His_{10}, we monitored the kinetics of competitive binding to MCH. Here, we made use of dual-channel TIRFS to detect the binding of both ligands simultaneously in a time-resolved manner. TIRFS enables the time-resolved recording of surface-bound fluorescence.

A tris-NTA/biotin conjugate (^{BT}tris-NTA; Figure 6A) was loaded onto a streptavidin-functionalised surface.[18] The interactions of His_6- and His_{10}-tagged maltose binding proteins (MBPs) labelled with Oregon Green 488 (^{OG488}MBP-His_6) and with Cy5 (^{Cy5}MBP-His_{10}), respectively, with ^{BT}tris-NTA-loaded streptavidin were probed in real time by dual-colour TIRFS detection under flow-through conditions. In this and our previous studies, MBP was selected as a protein for the expression of oligohistidine-tagged proteins because of its high yield, the

 © 2009 Wiley-VCH Verlag GmbH & Co. KGaA, Weinheim

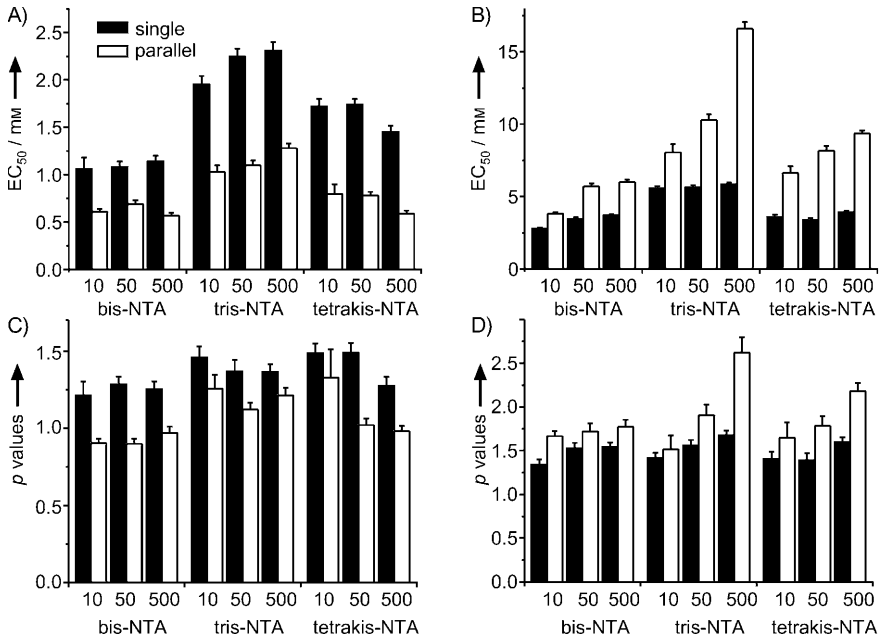

Figure 4. Effect of the presence of the corresponding other peptide on A), B) the EC_{50} and C), D) the *p* values of imidazole titration curves of A), C) His_6 and B), D) His_{10}. Black bars: noncompetitive binding of His_6 and His_{10}. Open bars: competitive binding of His_6 and His_{10}. The MCHs were spotted from 10 to 500 μM solutions; EC_{50} and *p* values for three concentrations are shown. Peptides were used at a concentration of 20 nM each.

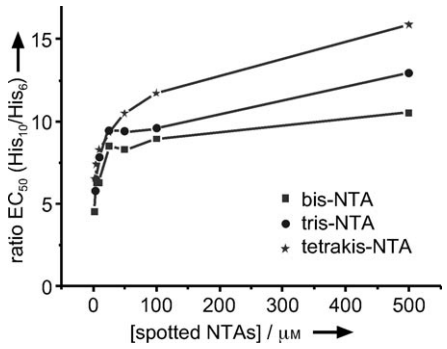

Figure 5. Dependence of selectivity (His_{10}/His_6 ratio) on the chelator head and the chelator density. Ratios were calculated from the data shown in Figure 4, including those spots that were omitted from Figure 4.

absence of cysteines and the availability of alternative means of purification. A cysteine residue for site-directed fluorescent labelling was introduced through an F391C mutation.

Binding curves for noncompetitive (presence of only one peptide) and for competitive binding (both ligands present simultaneously) of ^{OG488}MBP-His_6 and ^{Cy5}MBP-His_{10} in the presence of different concentrations of imidazole are shown in Figure 6B and C. Under noncompetitive conditions and in the absence of imidazole, similar binding kinetics were observed for ^{OG488}MBP-His_6 and ^{Cy5}MBP-His_{10}. Substantial differences in the binding amplitudes were obtained at different imidazole concentrations, which is in line with the different binding affinities of His_6 and His_{10}. Competitive binding of both ^{OG488}MBP-His_6 and ^{Cy5}MBP-His_{10}, however, yielded binding curves for ^{OG488}MBP-His_6 (but not ^{Cy5}MBP-His_{10}) in which an initial increase in binding was followed by a significant decrease in signal throughout the injection (Figure 6B, C). We explain this effect in terms of an active exchange of ^{OG488}MBP-His_6 by ^{Cy5}MBP-His_{10}, because His_{10} can better exploit the increased number of coordination sites generated by surface multivalency. In the absence of imidazole, the total binding of ^{Cy5}MBP-His_{10} to the surface was also somewhat reduced for competitive binding relative to noncompetitive binding, but this effect decreased with increasing imidazole concentration.

As a measure of selectivity, the ratios of the signals for ^{Cy5}MBP-His_{10} and ^{OG488}MBP-His_6 during the injection were plotted. Strikingly, an increase in the ratio with time was observed in the case of competitive binding (Figure 6D), which we ascribe to the displacement of His_6 by His_{10}. Moreover, the ^{Cy5}MBP-His_{10}/^{OG488}MBP-His_6 ratios increased with increasing imidazole concentration, which is mainly due to the strong decrease in the signal for MBP-His_6. Consistent with the equilibrium microarray experiments, the relative binding of His_{10} and His_6 differed much more strongly when both ligands were present, relative to the surface loading observed when only one ligand was present (Figure 6E). Interestingly, similar ratios of initial binding rates between ^{OG488}MBP-His_{10} and ^{Cy5}MBP-His_6 over a large range of imidazole concentrations were observed under both competitive and noncompetitive conditions (Figure 6F), suggesting a transition from kinetic to thermodynamically controlled binding during the injection period.

Discussion

Multivalent interaction at interfaces is a complex phenomenon governed by a variety of parameters. By using the binding of oligohistidine peptides to arrays of different MCHs spotted at various densities, we have explored the contributions of molecular and surface multivalency to the generation of selectivity in the presence of a monovalent competitor. Our results reveal new and surprising characteristics of multivalent interactions at interfaces that greatly enhance the selectivity for the recognition of two oligohistidine peptides of different lengths.

For each ligand alone, the imidazole concentrations required to induce release of the peptide from the surface showed little dependence on the density of the chelator. One may argue that the immobilisation of MCHs by nanospotting had led to only small differences in surface density. However, the strong concentration dependence of binding when both ligands were

 © 2009 Wiley-VCH Verlag GmbH & Co. KGaA, Weinheim

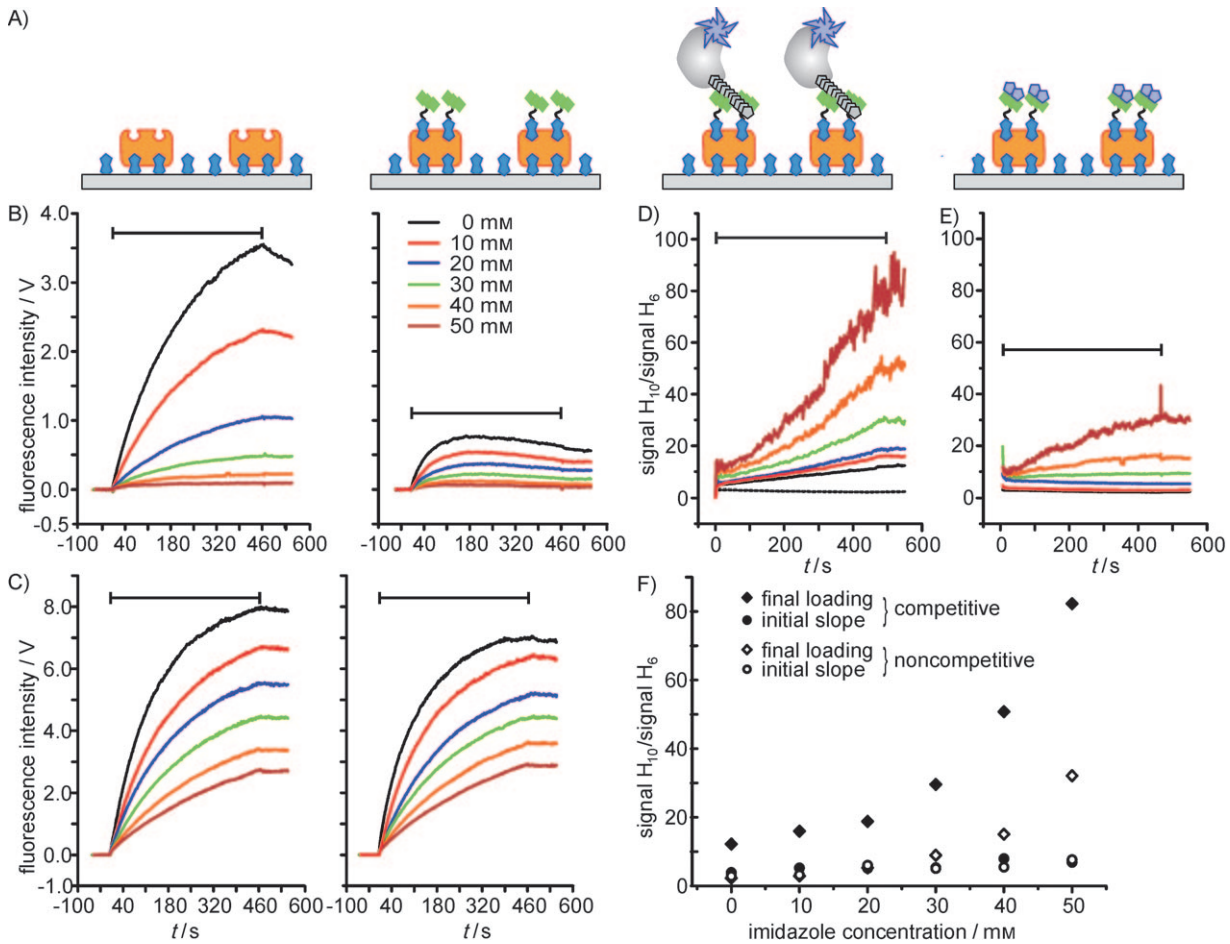

Figure 6. Competition kinetics of ^{OG488}MBP-His$_6$ and ^{Cy5}MBP-His$_{10}$ on ^{BT}tris-NTA/streptavidin as measured by dual-channel TIRFS detection. A) Cartoon demonstrating the experiment under noncompetitive conditions. After loading of a biotinylated surface with streptavidin, the free biotin binding sites were loaded with ^{BT}tris-NTA. Subsequently, the association and imidazole-induced dissociation kinetics of fluorescently labelled MBP were measured. B) Binding of ^{OG488}MBP-His$_6$ (500 nM) alone (left) and of ^{OG488}MBP-His$_6$ (500 nM) in the presence of ^{Cy5}MBP-His$_{10}$ (500 nM, right) at different imidazole concentrations (colour coding given in the legend; the bar marks the injection period). C) ^{Cy5}MBP-His$_{10}$ (500 nM) alone (left) and ^{Cy5}MBP-His$_{10}$ (500 nM) in the presence of ^{OG488}MBP-His$_6$ (500 nM, right) at different imidazole concentrations (same colour coding as B)). D), E) Time dependence of selectivity for ^{Cy5}MBP-His$_{10}$ over ^{OG488}MBP-His$_6$ for D) competitive and E) noncompetitive binding. D) Simultaneous injection of both ligands at a concentration of 500 nM in the absence or presence of different imidazole concentrations [dotted line: no competition, no imidazole (that is, both ligands measured separately), same colour coding as B)]. E) Injection of both ligands individually; this means that in D) ratios were calculated from signals recorded simultaneously by dual-channel TIRFS whereas in E) ratios were derived from signals recorded in pairs of experiments. F) ^{Cy5}MBP-His$_{10}$/^{OG488}MBP-His$_6$ ratios as determined from the final loading and initial slopes of the binding curves as a function of imidazole concentration for competitive and noncompetitive binding.

present over the whole range of spotted concentrations clearly indicates that the spots differed in ligand density.

The EC_{50} values increased with chelator multivalency on going from mono- to tris-NTA. For tetrakis-NTA, EC_{50} values were similar to those for tris-NTA, which we have observed previously (A.R. and J.P., unpublished results). Nevertheless, independent of the nature of the chelator and the chelator density, the imidazole concentrations required to induce half-maximum release were about 2.5 times higher for His$_{10}$ than those required for His$_6$. Although the general observations with respect to chelator- and density-dependence of binding compared very favourably with those reported before, we nevertheless noticed that previously a higher dependence on MCH density had been found.[8] Moreover, larger *p* values and a stronger dependence on the nature of the MCH had been observed.[10] These differences probably have to be ascribed to the stopped-flow format used in our microarray experiments, resulting in equilibrium binding, in comparison to the flow-through format used in previously published analyses.

Remarkably, very different EC_{50} values were obtained for His$_6$ and His$_{10}$ under competitive conditions, demonstrating that the ligands had been mutually affecting one another. For the low-affinity ligand His$_6$ in the presence of His$_{10}$, the EC_{50} values decreased even further, whereas for His$_{10}$ the EC_{50} values increased. This increase was strongly dependent on chelator density and the nature of the chelator. In contrast, for His$_6$ the EC_{50} values remained largely independent on surface density or even showed a slight decrease.

The lower EC_{50} value for the His$_6$ peptide may be considered a logical consequence of a lower concentration of surface-bound peptide according to Cheng–Prusoff.[21] However, because the surface concentration of His$_{10}$ should also be lower in the presence of the hexahistidine, the higher EC_{50} value for His$_{10}$ was very surprising.

 © 2009 Wiley-VCH Verlag GmbH & Co. KGaA, Weinheim

We propose a statistic distribution of the MCHs on the surface as the molecular basis for this striking behaviour. This distribution leads to binding sites with different surface multivalencies. Because of its greater number of histidine side chains, His_{10} can better exploit surface multivalency than His_6. Upon competitive binding of His_6 and His_{10}, we believe that these peptides are targeted into binding sites with different multivalencies (Scheme 2): His_{10} competes with His_6 much more successfully for binding sites with high surface multivalency, and is therefore enriched in these. The higher the surface loading with MCHs, the larger the number of such high-multivalency binding sites. In support of this hypothesis, real-time fluorescence detection of competitive binding kinetics of both peptides revealed an initial phase of rapid His_6 binding followed by a partial dissociation of His_6 indicative of a transition from kinetically to thermodynamically controlled binding. We explain this observation in terms of an active displacement of His_6 by docking of His_{10} to excess coordination sites in the vicinity. Conversely, the displacement of His_{10} by His_6 is much less likely, because His_{10} occupies more coordination sites. Therefore, the exchange of His_6 for His_{10} is particularly efficient at sites with high surface multivalencies, resulting in a preferred targeting of His_{10} in high-affinity binding sites and therefore increased EC_{50} value for elution with imidazole.

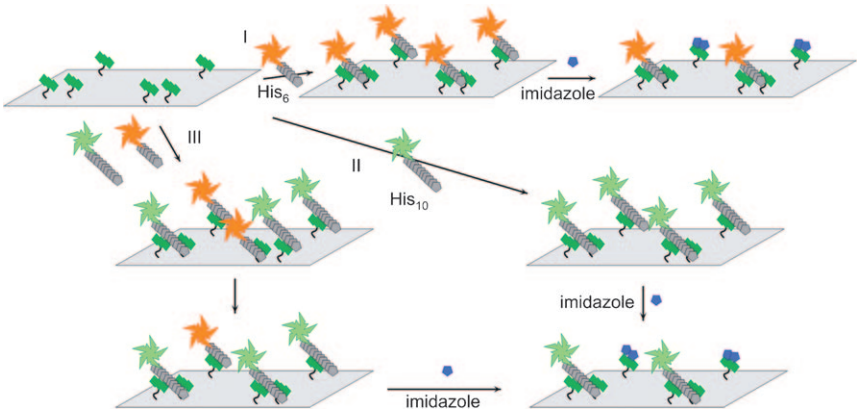

Scheme 2. Heterogeneous surface multivalency and sorting of His_6 and His_{10} under competing conditions. Details in the text.

This sorting mechanism could also explain the increased *p* values of the titration curves under competing conditions. Dissociation of peptide over a smaller range of imidazole concentrations reflects an increased homogeneity of binding sites. With increasing density of MCHs on the surface, the surface multivalency also increases, explaining why the His_{10}/His_6 ratio increases with the surface concentration of the MCH.

However, we did not find clear evidence for an active role of imidazole in the displacement of His_6 by His_{10}, because no accelerated displacement of His_6 at higher imidazole concentrations was observed. Rather, the monovalent competitor reduced the binding affinity for His_6 more strongly than for His_{10}, thus enhancing the contrast upon competitive binding.

The results presented in this paper shed light on the complexity of competitive multivalent interactions at interfaces, which is highly relevant for quantitative understanding of numerous fundamental biological mechanisms. With respect to the general characteristics of multivalent systems, our results show that selectivity might not originate from the binding of an individual ligand when considered in isolation. Furthermore, these insights into the selective recognition of different oligohistidine ligands further widen the scope of applications of the oligohistidine recognition system in the controlled manipulation of biomolecules.

Experimental Section

Reagents: Standard chemicals and solvents were from Fluka (Neu-Ulm, Germany), Lancaster, (Mülheim am Main, Germany), Acros (Ulm, Germany), Fisher Scientific (Loughborough, UK), J.T. Baker (Deventer, The Netherlands), Biosolve (Valkensvaard, The Netherlands) and Sigma–Aldrich (Steinheim, Germany). Solvents were in p.a. quality, LiChrosolv Gradient Grade and Uvasol (for HPLC and MS). Deionised water was used for washing glass surfaces and as system liquid for the nanopipettor. Chemicals for the derivatisation of the glass surfaces were from ABCR (Karlsruhe, Germany), Fluka (Deisenhofen, Germany) and Sigma–Aldrich. Carboxyfluorescein was from Fluka (Neu-Ulm), S0387 from FEW-Chemicals (Wolfen, Germany), Oregon Green from Invitrogen (Karlsruhe, Germany), Atto565 from Atto-Tec (Siegen, Germany) and Cy5 from GE Healthcare (Freiburg, Germany).

Peptide synthesis: Oligohistidine peptides were synthesised on TCP-resin by automated peptide synthesis with solid-phase Fmoc/*t*Bu-chemistry on an automated peptide synthesiser for multiple peptide synthesis (RSP5032, Tecan, Hombrechtlikon, Switzerland) in 2 mL syringes as described previously.[16] Amino acids were coupled in tenfold excess by DIC/HOBt coupling. Fluorescent labelling proceeded with the side chain-protected peptide on the resin. To ensure complete removal of the N-terminal Fmoc protecting group, the resin was washed with piperidine in DMF (20%, *v*/*v*) for 10 min. 5(6)-Carboxyfluorescein (Fluo, 5 equiv) was coupled with DIC/HOBt (5 equiv each) in DMF for 16 h, S0387 (3 equiv) with DIC/HOBt (6 equiv each) in DMF for 16 h.

For 5(6)-carboxyfluorescein, prior to cleavage, fluorescein oligomers resulting from acylation of the phenolic hydroxy group of the fluorescein moiety were removed by washing the resin in flow through with piperidine/DMF (1:4). For the S0387-labelled peptide, the resin was first washed four times with acetic acid in DMF (1%, *v*/*v*). Then, the resins were washed three times each with DMF, MeOH, DCM and diethyl ether. The purities of all peptides were determined by analytical HPLC. The identities of the peptides were confirmed by MALDI-TOF MS analysis. Peptides with a purity of less than 85% were purified by preparative HPLC. All peptides used were $>95\%$ pure (214 nm HPLC).

Protein expression and purification: Maltose-binding proteins with C-terminal hexahistidine (MBP-His_6) and decahistidine (MBP-

 © 2009 Wiley-VCH Verlag GmbH & Co. KGaA, Weinheim

His_{10}) tags were cloned by insertion of the corresponding linker into the multiple cloning site of the vector pMALc2x (New England Biolabs). For cysteine-specific labelling of MBP-His_{10}, F391 within the linker region between the MBP and the H_{10}-tag was mutated into a cysteine by ligase chain reaction. The proteins were expressed in *Escherichia coli* and purified by immobilised metal affinity chromatography followed by size exclusion chromatography as described previously.[10] The MBP-His_6 was labelled with Oregon Green 488 (OG488) *N*-hydroxysuccinimidyl ester in HEPES-buffered saline (HBS; 20 mM Hepes, pH 7.5, 150 mM sodium chloride) by standard protocols. The concentrations of protein and the reactive dye were optimised so that an average labelling degree of ~1 was obtained as determined photometrically: MBP-His_{10} F391C was treated with Cy5 maleimide (twofold molar excess) in HBS by standard protocols. The labelled proteins (^{OG488}MBP-His_6 and ^{Cy5}MBP-His_{10}) were separated from the free fluorophore and aggregates by size exclusion chromatography.

Preparation of MCH microarrays: The MCHs were synthesised as described before.[9] MCH microarrays were generated on type 1, BK7 coverslips of 12 mm diameter (Marienfeld, Lauda-Königshofen, Germany). Prior to surface functionalisation, coverslips were immersed in acetone for 15 min, followed by incubation for 16 h in freshly prepared Piranha solution (H_2SO_4/30% H_2O_2 6:5, *v/v*). The coverslips were then rinsed thoroughly with doubly distilled H_2O (ddH_2O) and dried in a stream of filtered process air, and were then either used immediately for further treatment or stored under argon. For epoxy activation, coverslips were incubated with (3-glycidyloxypropyl)trimethoxysilane (GOPTS) for 8 h at room temperature followed by careful rinsing with acetone and drying.

For succinimidyl ester activation, coverslips were incubated with 3-aminopropyltriethoxysilane (3%, *v/v*) in ethanol/H_2O (95:5, *v/v*) for 1 h at room temperature. The reaction was stopped by dilution with ethanol followed by thorough rinsing of the coverslips with ethanol and heating of the coverslips at 115 °C for 1 h. Next, the coverslips were rinsed with ethanol again and dried in a stream of filtered process air. Finally, the coverslips were incubated with a solution of suberic acid bis(*N*-hydroxysuccinimidyl ester) (35 mM) and DIPEA (82.5 mM) in DMF for 2.5 h. The coverslips were then rinsed with DMF, dried in a stream of filtered process air and used immediately for the generation of microarrays.

Microarrays were spotted with the aid of a piezo-electric contact-free nanopipettor (Nanoplotter NP2.0, GeSiM, Dresden, Germany), mounted in a housing with humidity control. The spotted volume was 0.9 nL per spot. C-Ahx-K(Fluo)-NH_2 (Ahx, 6-aminohexanoic acid) was spotted as a control for surface functionalisation. The control peptide was dissolved to a concentration of 50 μM in DMF/NH_4Ac (10 mM)/buffer (1:4, *v/v*; pH 7.3), and the MCHs were dissolved in ddH_2O and diluted in NH_4Ac buffer (10 mM, pH 7.3) to the indicated concentrations. The coverslips were placed on a cool plate, and the relative humidity and temperature of the plate were adjusted to just above dew point. After spotting, the arrays were left on the cool plate for 1 h, followed by drying and thorough washing with DMF (1 h), acetone (1 h), HBS (HEPES (10 mM), NaCl (135 mM), KCl (5 mM), $MgCl_2$ (1 mM), $CaCl_2$ (1.8 mM), pH 7.3; 16 h) and ddH_2O (1 h) and dried in a stream of filtered process air.

Imidazole titration experiments: Dissociation curves of fluorescently labelled oligohistidines were derived from fluorescence images recorded by confocal laser scanning microscopy with an inverted LSM510 confocal microscope (Carl Zeiss, Göttingen) and a Plan Neofluar 10×0.3 NA objective. The confocal detection served for the suppression of out-of-focus fluorescence of free peptides in the buffer. Fluorescein and S0387 fluorescence were simultaneously detected by excitation with the 488 nm line of an argon-ion laser and a 633 nm helium–neon laser and detection of fluorescence with a BP505–550 band-pass filter and an LP650 long-pass filter. Fluorescence of both channels was separated with an NFT570 dichroic mirror. The detector and amplifier settings enabled the saturation-free recording of fluorescence for the whole microarray and for the full concentration range of the peptides. Microarrays were imaged by scanning of individual frames in a mosaic-like fashion.

For the measurement of titration curves, coverslips were mounted in a custom-made holder.[12] Prior to the incubation with oligohistidines, coverslips were washed with EDTA (10 mM, 1 mL) for 10 min, dried and incubated with a solution of $NiCl_2$ (10 mM) for 10 min. Following a quick rinse with water, the array was incubated with a solution of fluorescently labelled oligohistidines (1 mL) for 30 min. The solution was agitated by pipetting on the array several times during this period. After recording of an initial image of the array, the MCH-bound ligands were titrated by stepwise addition of imidazole solution (0.5 M) to cover a concentration range of 0.5 to 10 μM. Each addition was followed by careful mixing for 4.5 min and image acquisition. This procedure was repeated until there was no further decrease in spot intensity. In order to facilitate direct visual comparison of titration curves, the titration curves were normalised. Firstly the fluorescence at the end of the titration was subtracted, thereby removing offset due to background fluorescence. Background fluorescence was due to some unspecific binding of the peptides to the spots (Figure S2) and out-of-focus fluorescence that was not fully suppressed by the confocal detection. As a consequence, fitting of the titration curves was performed in offset-free manner. The curves then were normalised on the basis of the background-corrected intensities in the absence of imidazole. Titration curves for titrations with imidazole were fitted as described previously with a logistic sigmoidal function [Eq. (1)].

$$R_{\text{trapped}}(c) = \frac{R_{\text{trapped,max}}}{1 + (c/\text{EC}_{50})^p} \quad (1)$$

R_{trapped} denotes the bound oligohistidine at equilibrium in the presence of a given imidazole concentration *c*. $R_{\text{trapped,max}}$ is the maximum attainable signal in the absence of imidazole, and EC_{50} the imidazole concentration for half-maximum binding of oligohistidine peptide. The exponent *p* represents different slopes of the titration curve that qualitatively are a result of different modes of binding.

Image analysis: Array images were analysed with Array-Pro Analyzer Version 4.5.1.48 (Media Cybernetics, Silver Spring, MD, USA) with use of the confocal images without any pre-processing. Signals were corrected for local background, corresponding to a ring around each spot. This background contained contributions from surface-bound fluorescence as well as fluorescence of free peptide in the incubation buffer. For each pair of spots the average was calculated. Dissociation curves were fitted and EC_{50} values determined by use of Microcal Origin 6.1 (OriginLab Corporation, MA, USA).

Real-time kinetics by total internal reflection fluorescence spectroscopy: Competition on surfaces was monitored in real time by dual-colour total internal reflection fluorescence spectroscopy (TIRFS) with simultaneous label-free detection by reflectance interference (RIf) as reported earlier.[15] OG488 and Cy5 fluorescence were excited simultaneously with an argon ion laser (488 nm) and a helium–neon laser (633 nm). For protein immobilisation, the

 © 2009 Wiley-VCH Verlag GmbH & Co. KGaA, Weinheim

transducer surface was covered with a PEG polymer brush to prevent nonspecific adsorption,[17] and biotin was covalently attached as described recently.[18] All binding experiments were carried out in Hepes buffer [HEPES (20 mM), NaCl (150 mM), Triton X100 (0.01 %), pH 7.5] by use of a flow-through system as described.[15] Firstly, streptavidin (100 nM) was immobilised on the biotinylated surface and the remaining biotin binding sites were loaded with ^{BT}tris-NTA (100 nM). For probing of competitive binding, ^{Cy5}MBP-His$_{10}$ (500 nM) and ^{OG488}MBP-His$_6$ (500 nM) were injected simultaneously at different imidazole concentrations (0–50 mM), and both the fluorescence signals and the RIf signals were recorded. As a reference, ^{Cy5}MBP-His$_{10}$ (500 nM) and ^{OG488}MBP-His$_6$ (500 nM) were immobilised separately at different imidazole concentrations (0–50 mM). The absolute surface concentrations of both proteins were comparable, as confirmed by the RIf signals.

Acknowledgements

This work was supported in the Nanobiotechnology initiative of the German Ministry of Education and Research (BMBF, grant number 0312005). R.B. gratefully acknowledges support from the Volkswagen Foundation ("Nachwuchsgruppen an Universitäten", I/77 472). J.P. was a Heisenberg Professor funded by the Deutsche Forschungsgemeinschaft (PI405/5).

Keywords: fluorescence · microarrays · multivalency · receptors · selectivity

[1] R. T. Lee, Y. C. Lee, *Glycoconjugate J.* **2000**, *17*, 543–551.
[2] J. Rao, J. Lahiri, L. Isaacs, R. M. Weis, G. M. Whitesides, *Science* **1998**, *280*, 708–711.
[3] P. I. Kitov, D. R. Bundle, *J. Am. Chem. Soc.* **2003**, *125*, 16271–16284.
[4] a) M. Mammen, S. K. Choi, G. M. Whitesides, *Angew. Chem.* **1998**, *110*, 2908–2953; *Angew. Chem. Int. Ed.* **1998**, *37*, 2754–2794.
[5] J. Huskens, A. Mulder, T. Auletta, C. A. Nijhuis, M. J. Ludden, D. N. Reinhoudt, *J. Am. Chem. Soc.* **2004**, *126*, 6784–6797.
[6] J. Huskens, *Curr. Opin. Chem. Biol.* **2006**, *10*, 537–543.
[7] A. Tinazli, J. Tang, R. Valiokas, S. Picuric, S. Lata, J. Piehler, B. Liedberg, R. Tampe, *Chem. Eur. J.* **2005**, *11*, 5249–5259.
[8] R. Valiokas, G. Klenkar, A. Tinazli, R. Tampe, B. Liedberg, J. Piehler, *ChemBioChem* **2006**, *7*, 1325–1329.
[9] S. Lata, A. Reichel, R. Brock, R. Tampe, J. Piehler, *J. Am. Chem. Soc.* **2005**, *127*, 10205–10215.
[10] S. Lata, J. Piehler, *Anal. Chem.* **2005**, *77*, 1096–1105.
[11] S. Lata, M. Gavutis, R. Tampe, J. Piehler, *J. Am. Chem. Soc.* **2006**, *128*, 2365–2372.
[12] M. Elbs, R. Brock, *Anal. Chem.* **2003**, *75*, 4793–4800.
[13] M. Elbs, M. Hulko, J. Frauenfeld, R. Fischer, R. Brock, *Anal. Bioanal. Chem.* **2007**, *387*, 2017–2025.
[14] D. Axelrod, T. P. Burghardt, N. L. Thompson, *Annu. Rev. Biophys. Bioeng.* **1984**, *13*, 247–268.
[15] M. Gavutis, S. Lata, P. Lamken, P. Muller, J. Piehler, *Biophys. J.* **2005**, *88*, 4289–4302.
[16] R. Fischer, O. Mader, G. Jung, R. Brock, *Bioconjugate Chem.* **2003**, *14*, 653–660.
[17] J. Piehler, A. Brecht, R. Valiokas, B. Liedberg, G. Gauglitz, *Biosens. Bioelectron.* **2000**, *15*, 473–481.
[18] A. Reichel, D. Schaible, N. Al Furoukh, M. Cohen, G. Schreiber, J. Piehler, *Anal. Chem.* **2007**, *79*, 8590–8600.
[19] P. Angenendt, J. Glokler, J. Sobek, H. Lehrach, D. J. Cahill, *J. Chromatogr. A* **2003**, *1009*, 97–104.
[20] O. Mader, K. Reiner, H.-J. Egelhaaf, R. Fischer, R. Brock, *Bioconjugate Chem.* **2004**, *15*, 70–78.
[21] Y. Cheng, W. H. Prusoff, *Biochem. Pharmacol.* **1973**, *22*, 3099–3108.

Received: January 2, 2009
Published online on June 29, 2009

 © 2009 Wiley-VCH Verlag GmbH & Co. KGaA, Weinheim